Interfaces in graded coatings on titanium-based implants

S. Lopez-Esteban, C.F. Gutierrez-Gonzalez, Laurent Gremillard, E. Saiz, A.P. Tomsia

Published in final edited form as:
J Biomed Mater Res A. 2009 March 15; 88(4): 1010–1021. doi:10.1002/jbm.a.31935.

Interfaces in graded coatings on titanium-based implants

S. Lopez-Esteban[1,2,*], **C. F. Gutierrez-Gonzalez**[1,2], **L. Gremillard**[1,3], **E. Saiz**[1], and **A. P. Tomsia**[1]

[1]Materials Sciences Division, 62R0203, Lawrence Berkeley National Laboratory, Berkeley, California 94720, USA

[2]Materiales Particulados, Instituto de Ciencia de Materiales de Madrid, Consejo Superior de Investigaciones Científicas (CSIC), Cantoblanco, 28049 Madrid, Spain

[3]Université de Lyon, INSA-Lyon, MATEIS, UMR CNRS 5510, 20 avenue Albert Einstein, Villeurbanne F-69621, France

Abstract

Graded bilayered glass-ceramic composite coatings on Ti6Al4V substrates were fabricated using an enameling technique. The layers consisted of a mixture of glasses in the CaO-MgO-Na_2O-K_2O-P_2O_5 system with different amounts of calcium phosphates (CPs). Optimum firing conditions have been determined for the fabrication of coatings having good adhesion to the metal, while avoiding deleterious reactions between the glass and the ceramic particles. The final coatings do not crack or delaminate. The use of high-silica layers (>60 wt % SiO_2) in contact with the alloy promotes long-term stability of the coating; glass-metal adhesion is achieved through the formation of a nanostructured Ti_5Si_3 layer. A surface layer containing a mixture of a low-silica glass (~53 wt % SiO_2) and synthetic hydroxyapatite particles promotes the precipitation of new apatite during tests *in vitro*. The *in vitro* behavior of the coatings in simulated body fluid depends both on the composition of the glass matrix and the CP particles, and is strongly affected by the coating design and the firing conditions.

Keywords

glass coating; enameling; titanium alloy; calcium phosphate; bioactivity; hydroxyapatite

INTRODUCTION

Coatings with variable solubility can better match the requirements of an implant, depending on its function and location in the body. Hench proposed that the optimal solution to biomaterials problems would be to create a composite coating whose dissolution rates would match the repair rates of body tissues, which vary enormously depending upon the tissue type, age, and health.[1] A novel approach to provide a material that can meet all these physiological requirements, while being mechanically reliable, is to produce functionally graded glass composite coatings.

In recent works, the possibility of fabricating glass or ceramic coatings on metallic alloys using different techniques[2][3] such as plasma spraying[4], sol-gel,[5][6] biomimetic process,[7] magnetron sputtering,[8] radiofrequency sputtering,[8] electrophoretic

*Correspondence to S. Lopez-Esteban, Materials Sciences Division, 62R0203, Lawrence Berkeley National Laboratory, Berkeley, California 94720, USA S. Lopez-Esteban (slopez@icmm.csic.es).

deposition,[9][10] or a simple enameling technique[11–17] among others such as dip coating, physical vapor deposition, ion-beam, for instance, has been demonstrated. These graded glass layers can be modified by introducing calcium phosphate (CP) mixtures to control the dissolution rates. CPs, such as hydroxyapatite (HA), tricalcium phosphate and others, are currently in use in many biomedical applications that include the repair of bony and periodontal defects, ear and eye implants, spine fusion or coating for dental and orthopedic implants. Graded glass layers design can also be used to induce a faster generation of apatite at the interface bone/implant, such that rapid bonding with the bone can be expected.[18] The addition of CP particles should enhance the versatility of the coatings, as their resorption rates and bioactivity could be further adjusted by changing their composition, which would allow us to design implants for specific applications; this possibility makes these composites promising for coating materials for orthopedic and dental uses. For example, a combination of resorbable CP and HA phases in a graded coating may promote rapid fixation, limit total resorption, and provide a fracture-resistant interface. Indeed, Kasemo and Gold[19] wrote that the future of biomaterials must include the development of coatings with programmed dissolution of multilayer surfaces, which would provide new opportunities to optimize the biomaterial coating surface for different periods of the healing-in phase. Such coatings could expose different microarchitectures, chemical patterns, and porosities at different times.

The goal of the present work is to study the interfaces in graded glass-ceramic composite coatings on Ti6Al4V substrates obtained by an enameling technique. Three types of interfaces in this bilayered composite are investigated: (a) Ti alloy/glass, (b) glass/CP, and (c) glass/SBF (SBF, Simulated Body Fluid). The effect of the CP additions on the coating microstructure is analyzed compared to pure glass coatings. Different CPs in varying proportions have been added to produce materials with the potential of covering a wide spectrum of resorbability and capacity to promote the precipitation of new apatite during tests *in vitro*. Finally, the effect of the different CP additions on the *in vitro* behavior in SBF is also analyzed, in order to study the chemical and microstructural evolution of the coatings under conditions that simulate their biological interactions with the body. Because the solution-precipitation processes that occur on the coating surfaces have a determinant role on their bone-bonding mechanisms, studies in SBF provide fundamental data to predict and understand the *in vivo* behavior.[20]

MATERIALS AND METHODS

Glasses

Glasses were prepared following a standard procedure.[11] Appropriate reagents (SiO_2, Cerac, U.S., 99.5%, purity), $CaCO_3$ (JT Baker, U.S., 99.9%), MgO (JT Baker 98.6%), K_2CO_3 (Allied Chemical, U.S., 99%), $NaHCO_3$ (JT Baker 99.5%), and $NaPO_3$ (Allied Chemical 99.7%) were mixed in ethanol using a high-speed stirrer. The mixture was first dried at +80°C for 12 h, and then fired in air at temperatures ranging between 1400 and 1500°C for 4 h in a Pt crucible. The melt was cast into a graphite mold to obtain glass plates (~50 × 50 × 5 mm) that were subsequently milled in a planetary agate mill and sieved (75 μm).

The compositions and thermal properties of the glasses were investigated in Ref.[14] and are shown in Table I. CTE is the coefficient of thermal expansion, T_g is the glass transition temperature, and T_s is the softening point. All compositions have a P_2O_5 content fixed at 6 wt %, so they are named as 6P followed by their silica content in wt %. For instance, 6P64 stands for a glass with a 6 wt % P_2O_5 and 64 wt % silica. The size distribution of the powders was obtained using a sedimentation method (Horiba, model CAPA 700, Japan) resulting that 50 vol % of the glass particles have a diameter below 10.5 ± 0.1 μm.

Coatings

The Ti6Al4V plates (President Titanium & Steel Co., USA, 99.0% purity, 10 × 10 × 1 mm) were ground with silicon carbide paper (800 grit), polished with diamond paste down to 1-μm particle size (Struers Planopol polishing machine), and cleaned in acetone and ethanol before their use. The suspensions were prepared by dispersing 1.06 g of glass powder in 100 mL of ethanol using a sonicator. Bilayered coatings were fabricated by sequential deposition: the first layer consisted of a high-silica glass (either 6P61 or 6P64) in contact with the alloy, and the second layer a mixture of a lower-silica glass and CP particles [Fig. 1(a)]. Afterward, the coatings were dried in air at +75°C overnight, and fired to make the glass flow and adhere to the metal. The samples were fired in a dental furnace (Unitek Ultra-Mat, U.S.), following the firing conditions determined in a previous work.[13] Coatings with 6P64 glass in contact with the alloy were fired at 820°C, while those with 6P61 were fired at 800°C. Unless otherwise specified, the samples used for the *in vitro* tests were fired for 5 s at the required temperature according to the results discussed in Ref.[13]. The samples were introduced into the furnace preheated at 600–620°C in air followed by a simultaneous rough evacuation to 10 kPa, and heated at 40°C/min to the desired firing temperature.

The specimens and coatings prepared are described in Table II. In most cases, the glass used as the layer in contact with the metal is 6P64. For comparison purposes, some samples have been coated with a 6P61 layer in contact with the alloy. These glasses have high silica content, and their thermal expansion matches well with that of Ti6Al4V. The glass used in the outer layer is either 6P53B or 6P61. The amount of CP particles added was 0, 5, 10, or 15 wt % with respect to the total amount of glass. The CP particles added were HA (Alfa Aesar, U.S., 34.0–40.0% Ca, particle diameter <1 μm), tricalcium phosphate (β-TCP, Fluka, U.S., 96% purity, particle diameter <4 μm), and dicalcium phosphate anhydro (DCPA, Fluka 97%, particle diameter <4 μm).

Characterization

The phase distribution and microstructure of the as-preparedcoatings were analyzed by X-ray diffraction (XRD, Siemens D500, with Cu K_α radiation), optical microscopy, and scanning electron microscopy (SEM, on a DS130C microscope, Topcon) with associated calibrated energy dispersive analysis (EDS, DX-4 system, EDAX). The EDS system was calibrated using glasses and CPs of known composition.

The influence of the firing time on the microstructure and composition of the coatings was studied by XRD, optical microscopy, SEM-EDS, and by transmission electron microscopy (TEM).

To analyze the adherence of the coatings, the relative crack resistance was qualitatively evaluated by indentation. Vickers indentations on the glass-metal interfaces were performed on cross-sections polished down to 1 μm (Buehler Vibromet polishing machine) using loads up to 1 kg.

Three samples fired for 5, 20, and 30 s, respectively, were prepared for TEM using a conventional technique. The samples were cross-sectioned with a diamond saw (thickness ~100 μm), then two samples were glued on a TEM Cu ring (coatings facing each other), and the assembly was thinned by tripod polishing down to 20-μm thickness. Finally, the samples were ion-milled (Gatan Duomill, cooled by liquid N_2) to reach electron transparency. The TEM observations were made at 200 keV in a JEOL 200CX transmission electron microscope.

The *in vitro* response of the glasses was studied by immersing the specimens (area ~1 cm^2) in controlled volumes of SBF, at +36.5°C, for fixed periods of time up to 12 months. Table

III shows the SBF composition compared to that of human plasma. To analyze the effect of the amount of SBF in the static tests, the same assays were performed using 75 and 200 mL of SBF. After the periods of time specified in Figure 13, the samples were removed from the liquid, rinsed in distilled water, and dried in air for 24 h. The coating surfaces and polished cross-sections were analyzed using XRD and SEM-EDS. The effect of immersion in SBF on the adhesion of the coating to the alloy was evaluated using Vickers indentation.

RESULTS

Glass coating characterization

Using the optimum firing conditions for the glasses in contact with the alloy (6P61 or 6P64), [13] multilayered coatings were fabricated [Fig. 1(a)]. The coatings were dense, free of either gas bubbles or cracks, and did not delaminate after cooling [Fig. 1(b)]. The final thickness of the bilayered coatings ranged between ~100 and 150 μm. The SEM-EDS analysis indicated that the thickness of each individual layer ranged between 50 and 75 μm.

In the XRD analysis, a surface layer ~20 μm thick contributed to ~90% of the diffracted X-ray intensity.[21] The peaks that appear in the XRD of the starting coatings are due to partial crystallization of the glass during the fabrication and they are indexed in Figure 2. Only peaks corresponding to the original CPs and the crystallization products can be identified in the XRD pattern of a coating with a pure 6P53B surface layer (without CP additions) fired at 820°C (sample S4 in Table II). Peaks corresponding to sodium calcium phosphate ($2.4CaO{\cdot}0.6Na_2O{\cdot}P_2O_5$), sodium calcium silicate ($Na_2O{\cdot}3CaO{\cdot}2SiO_2$), as well as diopside [$CaMg(SiO_3)_2$] were identified. The amount of crystalline phases in the glass was less than 5 vol %. [13]

Figure 3 shows the XRD diffraction patterns of the coatings with and without addition of CP particles before and after being 1 month in SBF. Only in the case of the coatings with HA addition, the pattern presents appreciable changes on the peaks distribution and intensities with respect to the coatings as prepared.

Alloy/glass interface

A TEM study of the glass/alloy interface 6P61/Ti6Al4V showed the formation of a thin reaction layer mainly formed by Ti_5Si_3.[12] The layer was composed of two regions: a continuous polycrystalline film in contact with the alloy and, on top of it, a zone with isolated Ti_5Si_3 nanoparticles (~10–30 nm in diameter) dispersed in the glass matrix. As the firing time increased (5, 20, and 30 s), the thickness of the continuous layer did not change appreciably, while the number of nanoparticles increased considerably (Fig. 4). In indentations at the glass-metal interface on polished cross-sections of these coatings, cracks did not propagate along the interface, but rather tended to be driven into the glass (Fig. 5).

Glass/CP interface

No interdiffusion or interfacial reaction between the different CP particles and the glass could be observed in the cross-sectional analysis of the coatings (Fig. 6). This opens the possibility of using the enameling technique to fabricate graded composite coatings with controlled composition.

Glass surface in contact with SBF: *In vitro* response

Composition of the glass layers—The composition of the glass layer in contact with the metal did not affect the *in vitro* behavior of the coatings in SBF. Coatings with 6P64 and 6P61 layers in contact with the Ti alloy had similar behavior. However, the composition of the glass on the surface layer had a remarkable effect. After 4 months in SBF, the samples

whose surface layer was a mixture of the high-silica 6P61 glass plus HA (S3) appeared slightly corroded. A layer rich in Ca and P could be detected by EDS on the surface glass, but there was no evidence of precipitation of new phases. However, the microstructure of the coatings containing 5 wt % HA particles dispersed in a low-silica 6P53B glass on the surface layer (S1 and S2) clearly evolved with time in SBF. Figure 7 shows the evolution of the XRD patterns of S1 after being soaked in SBF for different times up to 12 months. After 3 days in SBF, an apatite layer had precipitated on the coating surface, as identified by SEMEDS (Fig. 8) and XRD. The apatite layer consisted of nanosized carbonated hydroxyapatite [HCA, $Ca_{10}(PO_4)_3(CO_3)_3(OH)_2$] crystals (50–100 nm) with flakelike morphology. The EDS analysis indicated that the apatite incorporates 1–3 wt % MgO in its structure.

Figure 9 shows coating S1 after 1 month in SBF. Four separate regions were distinguishable in the SEM-EDS analysis of the coatings' cross-sections: the 6P64 glass layer (~70 ± 3 μm thick) that remained attached to the alloy; the remaining 6P53B + 5 wt % HA layer (~60 ± 3-μm thick); a Si-rich layer (~20 ± 3-μm thick); and, finally, a region that corresponded to the precipitated apatite (~10 ± 3-μm thick).

Particle composition and concentration—Three different CPs were selected to study the influence of the particle composition (S1, S5, and S6 in Table II). In all samples, the surface layer consisted of a mixture of 5 wt % CP particles dispersed in 6P53B glass. A coating with no CP additions was used as a control (S4).

XRD showed the presence of the starting CP particles in all the coatings, even after 4 months in SBF. The surface of the coatings with DCPA (sample S5), β-TCP (sample S6), or with no CP particle additions (sample S4) changed only slightly after 1 month in SBF, and no apatite precipitated (Figs. 3 and 10). The surface composition of the corroded glass was similar in the three cases. Peaks corresponding to Si, Ca, and P could be observed in the EDS area analysis (Fig. 10).

In samples without CP (Fig. 11), isolated CP crystal aggregates (80–100 μm in diameter) were found after 6 months in SBF. In coatings containing β-TCP particles, some isolated apatite aggregates (~40–100 μm) could be observed on the surface of the corroded coating after 2 months in SBF; after 4 months, approximately half of the surface was covered by apatite. On the other hand, samples with DCPA particles showed no sign of apatite precipitation, even after 2 months in SBF. However, as shown in Figure 7, an HCA layer precipitated on the surface of the coating containing synthetic HA particles (sample S1) after 3 days in SBF. To study the effect of the amount of HA particles added to the coating, the behavior of samples containing 5 and 10 wt % HA (4 and 8 vol %, respectively) dispersed in a 6P53B matrix in the surface layer was compared (S1 and S7). No significant differences could be observed in the time required for apatite precipitation.

Firing conditions—Two graded coatings were prepared to study the effect of the firing time on the properties of the coatings. Samples with 5 wt % HA particles dispersed in 6P53B glass in the surface layer were fired at 820°C for 5 and 15 s (S1 and S8, respectively). SEM (Fig. 12) and XRD showed that the surface of the sample fired for 15 s appeared corroded, but no apatite precipitated after immersion in SBF for a period of 4 months. However, a continuous layer of apatite precipitates completely covered the surface of the sample fired for 5 s after only 3 days.

Static *in vitro* tests—The effect of the volume of SBF used in static *in vitro* tests was evaluated by comparing the evolution of samples S1 (5 wt % HA dispersed in 6P53B glass) after immersion in 200 or 75 mL SBF for times up to 12 months. The results corresponding

to the first 4 months are plotted in Figure 13. Glass corrosion was considerably faster in the samples immersed in 200 mL SBF. In these samples, the external 6P53B layer is corroded after 1 month in SBF, as shown in the SEM micrograph in Figure 13(a). In all cases, a continuous layer of precipitated apatite formed, but in the sample immersed in 75 mL SBF, new HCA precipitation stopped after ~1 month. In the sample immersed in 200 mL SBF, the thickness of the precipitated apatite layer increased continuously for up to 4 months (~50 μm); however, it eventually stopped increasing, and the average thickness of the precipitated apatite layer after 4 and 12 months were similar.

DISCUSSION

The firing conditions play a double role in the coating properties. First, the appropriate firing schedule for the preparation of coatings with optimum adhesion (lack of delamination or excessive interfacial reactions) needs to be established. Optimum adhesion is obtained when the interfacial reaction layer is kept at a thickness of 100–200 nm [Fig. 4(a)]. At the same time, firing time and temperature both control the response of the coating that is affected by interdiffusion between the glass layers, glass crystallization, and the reactions between glass and the synthetic CP particles. The diffusion coefficient of Na^+ in soda-lime-silicate glasses typically ranges between 10^{-6} and 10^{-7} cm^2/s at temperatures between 800 and 900°C, and is several orders of magnitude higher than it is for other components.[22]

Even for the short firing times used in this work, sodium interdiffusion was fast enough to generate a smooth Na_2O profile that changed the composition of the surface layer, decreasing its alkaline content.[11][23] Furthermore, the firing temperatures were optimized for the high-silica glass in contact with the alloy and well above the softening point of 6P53B, promoting its crystallization. Both phenomena, interdiffusion and crystallization enhanced the resistance of the 6P53B surface layer to corrosion and hampered its ability to precipitate apatite in SBF.[14] In consequence, a coating with a pure 6P53B glass surface (without CP additions) was not able to precipitate a continuous apatite layer even after 6 months in SBF (Fig. 10). No deleterious reaction between the CP particles and the glass was observed for the firing times and temperatures used in this work (Fig. 6). This agrees with previous analysis of the interface between HA and silicate glasses in samples fired under similar conditions.[12]

There are two main limitations affecting the amount of CP particles that can be added. First, the upper limit is such that the glass/ceramic layer will not flow adequately during the enameling process, hampering the densification and adhesion of the coating. Second, the CP particles thermal expansion is of the order of $15 \times 10^{-6}°C^{-1}$, while for 6P53B glass, it is of the order of $11 \times 10^{-6}°C^{-1}$. Thus, the addition of CP particles will increase the thermal expansion of the surface layer and consequently increase the thermal stresses. Therefore, our results indicate that up to 10 wt % of CP particles (~1–10 μm in size) can be added to the surface layer without compromising processing and the mechanical stability of the coating.

The *in vitro* behavior of the coatings in SBF depended on both the composition of the glass matrix in the surface layer and on the composition and amount of CP particles. Glasses with silica contents above 60 wt % are very resistant to corrosion in aqueous environments and do not precipitate apatite during *in vitro* tests in SBF. Glasses with lower silica contents have a more open network structure that facilitates ion exchange with the solution, resulting in faster glass corrosion and precipitation of apatite as reported in detail for these glasses by Bloyer et al.,[15] following a path similar to that described by Hench[1] for Bioglass®. The steps involved are as follows: the exchange of Na^+ and K^+ from the glass with H^+ or H_3O^+ from solution, accompanied by the loss of soluble silica into the solution and the formation of silanols on the glass surface; condensation and repolymerization of a SiO_2-rich layer on

the surface; migration of Ca^{2+} and PO^{3-}_4 through the silica-rich layer forming a $CaO\text{-}P_2O_5$-rich film that incorporates calcium and phosphates from solution; finally, the crystallization of the amorphous CP film to form an apatite layer. It was shown[18] that the bioactive glass surface provided a substrate that was favorable to the rapid nucleation and growth of biologically equivalent HCA.

Other mechanisms of apatite nucleation and growing on apatite have been already described, proposing that new apatite can be nucleated on the top of the already-formed apatite layer.[24][25] When immersed in SBF, the apatite could reveal negative surface charge by exposing hydroxyl and phosphate units in its crystal structure. The apatite surface uses this negative charge to interact specifically with the positive calcium ions in the fluid, consequently forming a Ca-rich amorphous or nanocrystalline CP. The formation of this Ca-rich CP is assumed to take place in consecutive accumulation of the calcium ions, which makes it acquire and increase positive charge. The Ca-rich CP on the apatite, therefore, interacts specifically with the negative phosphate ions in the fluid to form a Ca-poor CP. This type of Ca-poor CP has been observed as a precursor, which eventually crystallizes into bonelike apatite on various bioactive ceramics.[18][26]

Excessive resorption of the coating might reduce mechanical fixation of the implant and also cause delamination, resulting in worn debris floating within the body and, ultimately, implant failure. The use of partially resorbable coatings may alleviate this potential problem, especially if the dissolution is achieved at a prescribed location.[27] During *in vitro* tests in SBF, both the particles and the glass could dissolve in the liquid. A way to manipulate the resorption rates and bioactivity of a glass composite coating is to mix glasses with diverse compositions and with different CPs. Different CPs have different degrees of solubility in water. At a pH of 7.5, the solubility isotherms of several CPs showed that the logarithmic products of the total molar Ca^{2+} concentration[28] ranged between 3.0 and 3.5 for DCPA, 3.5 and 4.0 for TCP, and 4.0 and 4.5 for HA. During *in vivo* testing, the solubility of TCP was reported to be more than 10 times higher than that of HA during the first weeks of implantation.[29] However, the dissolution rates depended considerably on the density and the crystallinity [30]: dense HA has a very low dissolution rate in neutral or alkaline aqueous solution; the dissolution rate can be considerably higher if the density or crystallinity is low.[30] In all cases, CP particles could be detected in the coating by XRD, even after 4 months in SBF.

The results of this work are consistent with the idea that synthetic HA particles act as nucleation centers, and promote the precipitation of new HCA during *in vitro* tests in SBF. The glass matrix also plays a role, since the presence of a low-silica glass (< 60 wt % SiO_2) and the associated ion exchange are still needed to promote HCA formation *in vitro*, even with HA additions. The effect of other CPs is limited, and the behaviors of the coatings without particles and those with β-TCP and DCPA are somewhat similar. In these cases, different degrees of dissoultion are observed and long periods of time are needed for the HA precipitation (2 months for samples with β-TCP, and 6 months with samples with no CP), and the precipitates never form a continuous layer. Samples containing DCPA do not precipitate new apatite at all.

The limitations associated with static *in vitro* testing are illustrated by the differences between the experiments performed using different volumes of SBF. The precipitated apatite crystals form a porous layer that does not stop the ionic exchange between the coating and the media. Larger volumes of SBF promote glass corrosion and HCA precipitation, but the apatite layer eventually comes to equilibrium with the dissolved ions in the surrounding solution. It should be pointed out that the inner high-silica layer in contact with the metal remains intact, maintaining good adhesion to the alloy, as could be expected since high-

silica glasses are resistant to corrosion in SBF. In indentation tests performed in the alloy/glass interface after "*in vitro*" test in SBF, the cracks traveled along the glass and did not propagate along the glass/metal interface (Fig. 14).

Different CPs present different degrees of solubility in aqueous solutions.[31] By adding different CPs to the glass coatings fabricated by enameling, we can further manipulate their solubility and *in vitro* and *in vivo* responses. The results of this work demonstrate that layers containing up to 10 wt % CP can be added without compromising their adhesion and coating integrity.

CONCLUSIONS

A simple enameling technique can be used for the fabrication of graded glass composite coatings on Ti-based alloys. The coatings consist of a high-silica glass layer in contact with the alloy to provide good adhesion, and a surface layer of low-silica glass with CP contents up to 10 wt %. The final coatings do not crack or delaminate. No deleterious reactions between the CPs and the glass occur during processing. The *in vitro* behavior in SBF depends strongly on the coating design and the firing conditions. By using different glasses and CPs, it is possible to manipulate the coating solubility and its *in vitro* and *in vivo* response. A surface layer consisting of synthetic HA particles dispersed in a low-silica glass matrix promotes apatite precipitation in SBF. Coatings containing other CPs do not promote *in vitro* apatite precipitation undergoing different degrees of dissolution and glass corrosion. In all cases, the high-silica layer in contact with the metal remains intact and maintains good adhesion even after 12 months in SBF, providing long-term stability. The results of this work demonstrate that enameling is a simple and versatile technique for the fabrication of glass/ceramic composite coatings on Ti6Al4V-based alloys. The use of different silicate glasses and CPs allows the fabrication of coatings with a wide range of solubility and bioactivity that can be tailored for specific applications.

Acknowledgments

The authors thank the LBNL National Center for Electron Microscopy for the use of the TEM facility. Laurent Gremillard was supported by the Regional Council of Rhone-Alpes and the Physical Metallurgy and Materials Sciences Group (GEMPPM, INSA Lyon, France). S. Lopez-Esteban was partly supported by a Fulbright grant and by the Spanish Ministry of Education and Science under Ramón y Cajal Program.

Funded by:

■ NIH/NIDCR; Grant Number: 1R01DE11289

REFERENCES

1. Hench LL. The story of bioglass. J Mater Sci Mater Med. 2006; 17:967–978. Links. [PubMed: 17122907]
2. Ma J, Chen CZ, Yao L, Bao QH. Characterization of some methods of preparation for bioactive glass coating on implants. Surf Rev Lett. 2006; 13:93–102. Links.
3. Zhao YF, Chen CZ, Wang DG. The current techniques for preparing bioglass coatings. Surf Rev Lett. 2005; 12:505–513. Links.
4. Yilmaz S, Ipek M, Celebi GF, Bindal C. The effect of bond coat on mechanical properties of plasma-sprayed Al_2O_3 and Al_2O_3-13 wt% TiO_2 coatings on AISI 316L stainless steel. Vacuum. 2005; 77:315–321. Links.
5. Li P, deGroot K, Kokubo T. Bioactive Ca-10$(PO_4)(6)(OH)_2$-TiO_2 composite coating prepared by sol-gel process. J Sol-Gel Sci Technol. 1996; 7:27–34. Links.

6. Milella E, Cosentino F, Licciulli A, Massaro C. Preparation and characterisation of titania/hydroxyapatite composite coatings obtained by sol-gel process. Biomaterials. 2001; 22:1425–1431. Links. [PubMed: 11336317]
7. Kokubo T, Kim HM, Kawashita M. Novel bioactive materials with different mechanical properties. Biomaterials. 2003; 24:2161–2175. Links. [PubMed: 12699652]
8. Schroeder A, Francz G, Bruinink A, Hauert R, Mayer J, Wintermantel E. Titanium containing amorphous hydrogenated carbon films (a-C : H/Ti): Surface analysis and evaluation of cellular reactions using bone marrow cell cultures in vitro. Biomaterials. 2000; 21:449–456. Links. [PubMed: 10674809]
9. Stojanovic D, Jokic B, Veljovic D, Petrovic R, Uskokovic PS, Janackovic D. Bioactive glass-apatite composite coating for titanium implant synthesized by electrophoretic deposition. J Eur Ceram Soc. 2007; 27:1595–1599. Links.
10. Boccaccini AR, Peters C, Roether JA, Eifler D, Misra SK, Minay EJ. Electrophoretic deposition of polyetheretherketone (PEEK) and PEEK/Bioglass (R) coatings on NiTi shape memory alloy wires. J Mater Sci. 2006; 41:8152–8159. Links.
11. Pazo A, Saiz E, Tomsia AP. Silicate glass coatings on Ti-based implants. Acta Mater. 1998; 46:2551–2558. Links.
12. Gomez-Vega JM, Saiz E, Tomsia AP, Oku T, Suganuma K, Marshall GW, Marshall SJ. Novel bioactive functionally graded coatings on Ti6Al4V. Adv Mater. 2000; 12:894–898. Links.
13. Gomez-Vega JM, Saiz E, Tomsia AP. Glass-based coatings for titanium implant alloy. J Biomed Mater Res. 1999; 46:549–559. Links. [PubMed: 10398016]
14. Lopez-Esteban S, Saiz E, Fujino S, Oku T, Suganuma K, Tomsia AP. Bioactive glass coatings for orthopedic metallic implants. J Eur Ceram Soc. 2003; 23:2921–2930. Links.
15. Bloyer DR, McNaney JM, Cannon RM, Saiz E, Tomsia AP, Ritchie RO. Stress-corrosion crack growth of Si-Na-K-Mg-Ca-P-O bioactive glasses in simulated human physiological environment. Biomaterials. 2007; 28:4901–4911. Links. [PubMed: 17714778]
16. Pavon J, Jimenez-Pique E, Anglada M, Lopez-Esteban S, Saiz E, Tomsia AP. Stress-corrosion cracking by indentation techniques of a glass coating on Ti6Al4V for biomedical applications. J Eur Ceram Soc. 2006; 26:1159–1169. Links.
17. Tomsia AP, Saiz E, Song J, Bertozzi CR. Biomimetic bonelike composites and novel bioactive glass coatings. Adv Eng Mater. 2005; 7:999–1004. Links.
18. Hench LL. Bioceramics: From concept to clinic. J Am Ceram Soc. 1991; 74:1487–1570. Links.
19. Kasemo B, Gold J. Implant surfaces and interface processes. Adv Dent Res. 1999; 13:8–20. Links. [PubMed: 11276751]
20. Kokubo T, Takadama H. How useful is SBF in predicting in vivo bone bioactivity? Biomaterials. 2006; 27:2907–2915. Links. [PubMed: 16448693]
21. *AbsorbDX V1.1.2.,* Program belonging to the software suite DiffracPlus Basic-Evaluation Part to calculate the depth of the layer analyzed by XRD in given conditions.
22. Kingery, WD.; Bowen, HK.; Uhlmann, DR. Introduction to Ceramics. Wiley; USA: 1960. p. 217-246.
23. Bloebaum RD, Beeks D, Dorr LD, Savory CG, DuPont JA, Hofmann AA. Complications with hydroxyapatite particulate separation in total hip arthroplasty. Clin Orthop Relat Res. 1994; 15:19–26. Links. [PubMed: 8118974]
24. Kim HM, Himeno T, Kokubo T, Nakamura T. Process and kinetics of bonelike apatite formation on sintered hydroxyapatite in a simulated body fluid. Biomaterials. 2005; 26:4366–4373. Links. [PubMed: 15701365]
25. Aparicio C, Manero JM, Conde F, Pegueroles M, Planell JA, Vallet-Regi M, Gil FJ. Acceleration of apatite nucleation on microrough bioactive titanium for bone-replacing implants. J Biomed Mater Res A. 2007; 82A:521–529. Links. [PubMed: 17295245]
26. Ohtsuki C, Kokubo T, Yamamuro T. Mechanism of apatite formation on CaO-SiO_2-P_2O_5 glasses in a simulated body-fluid. J Non-Cryst Solids. 1992; 143:84–92. Links.
27. De Bruijn JD, Flach JS, de Groot K, van Blitterswijk CA, Davies JE. Analysis of the bony interface with various types of hydroxyapatite in vitro. Cells Mater. 1993; 3:115–127. Links.

28. Nancollas, GH.; Zhang, J. Formation and dissolution mechanisms of calcium phosphates in aqueous systems. In: Brown, PW.; Constantz, B., editors. Hydroxyapatite and Related Materials. CRC Press; USA: 1994. p. 73-81.

29. Klein, CPAT.; Wolke, JGC.; de Groot, K. Stability of calcium phosphate ceramics and plasma spray coating. In: Hench, LL.; Wilson, J., editors. An Introduction to Bioceramics. World Scientific; Singapore: 1993. p. 199-221.

30. Varshneya, AK. Treatise on Materials Science and Technology. Tomozawa, M.; Doremus, RH., editors. Academic Press; USA: 1985. p. 242-306.

31. LeGeros, RZ.; LeGeros, JP. Dense hydroxyapatite. In: Hench, LL.; Wilson, J., editors. An Introduction to Bioceramics. World Scientific; Singapore: 1993. p. 139-180.

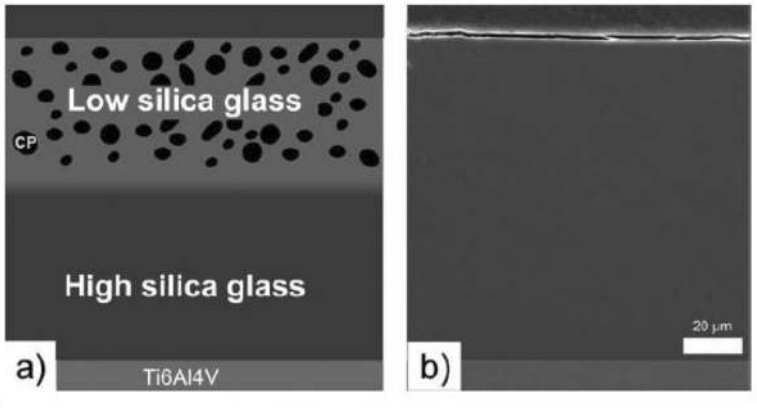

Figure 1.
(a) Schematic showing the design of the bilayered coatings, that is, a first layer of a high-silica glass in contact with the alloy and a second surface layer consisting of a mixture of a lower-silica glass and CP particles. (b) SEM micrograph of polished cross-section of sample S1, showing the glass density as well as the absence of gas bubbles or cracks.

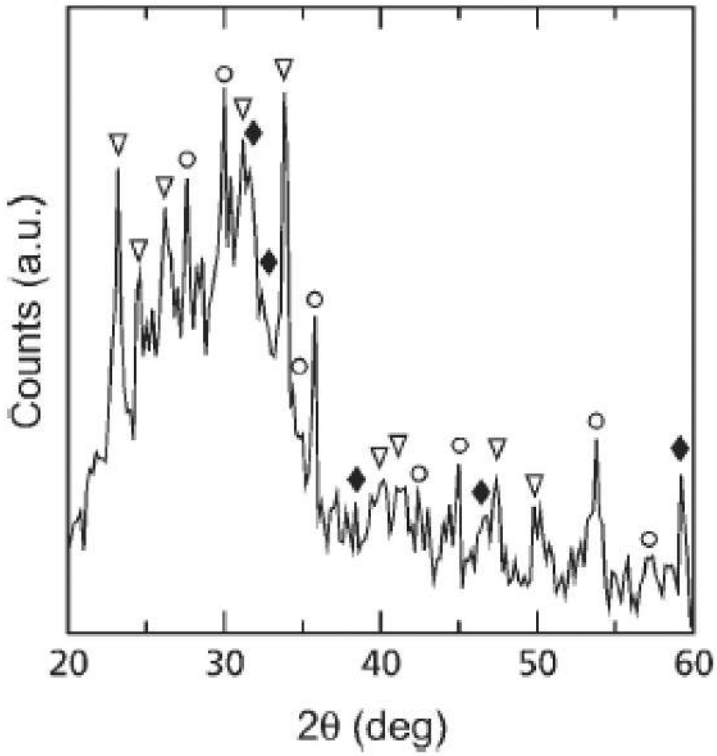

Figure 2.
XRD of the surface of S4 (glass surface layer 6P53B with no phosphate particles) showing the main crystalline phases found after firing: (▽) sodium calcium phosphate, (◆) sodium calcium silicate, and (◯) diopside.

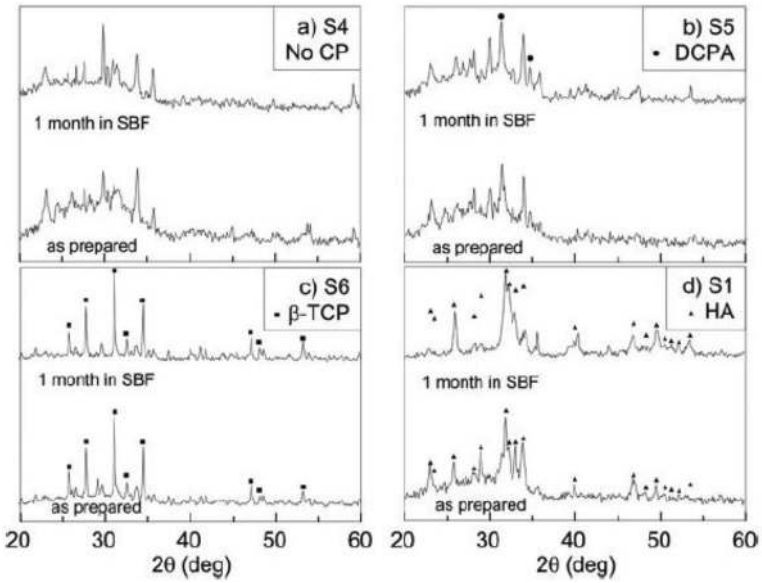

Figure 3.

XRD of the surface of different coatings with and without addition of CP particles. (a) has been added for comparison purposes and the corresponding peaks have been labeled in detail in Figure 2. In (b), the two peaks of DCPA have been labeled; the remaining peaks correspond to the glass surface. Peaks corresponding to β-TCP and HA are labeled in (c) and (d), respectively.

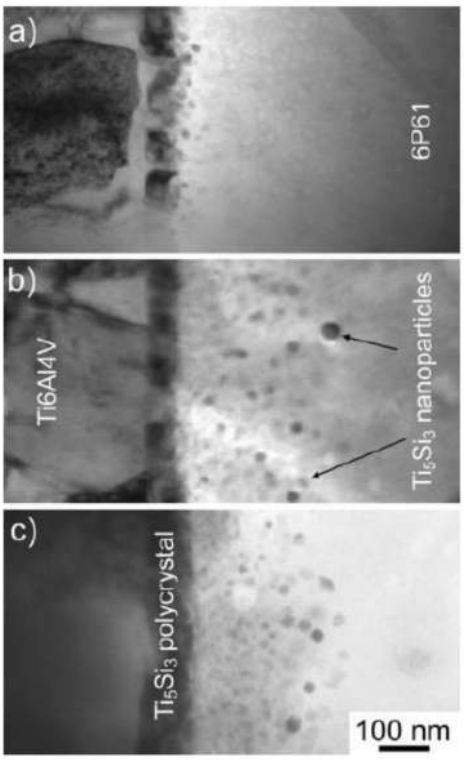

Figure 4.
TEM images of glass 6P61/Ti6Al4V interfaces annealed at 800°C for (a) 5 s, (b) 20 s, and (c) 30 s, respectively, showing the presence of a Ti_5Si_3 interfacial layer consisting of two regions: a continuous polycrystalline layer in contact with the alloy and a region with Ti_5Si_3 nanoparticles dispersed in the glass.

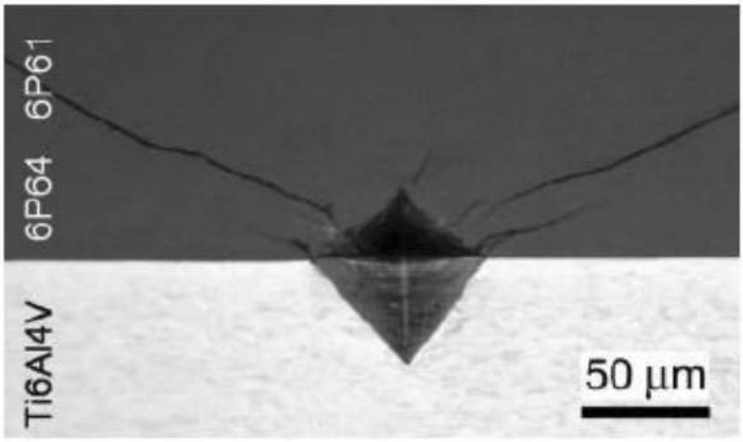

Figure 5.
Vickers indentation at the glass S3/Ti6Al4V interface performed using a 1-kg load in ambient air. The cracks do not propagate along the interface, but rather tend to be driven into the glass. The coating did not delaminate qualitatively indicating good glass-metal adhesion. The same behavior was found in all the samples.

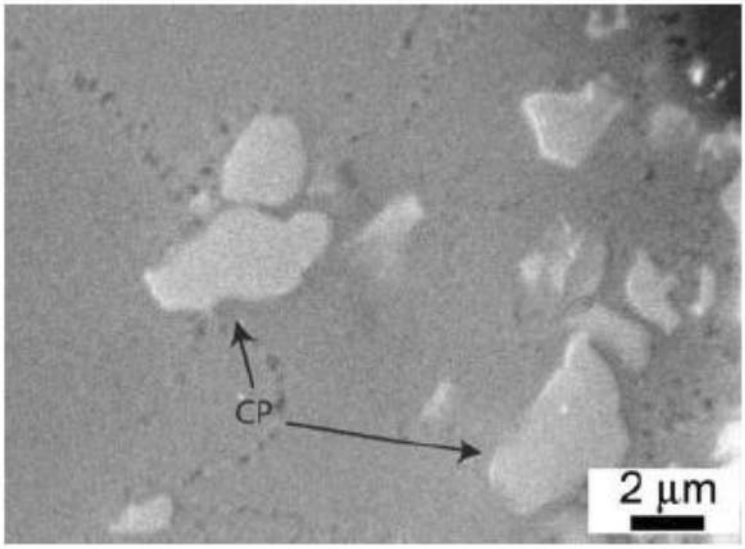

Figure 6.
Cross-section of sample S6 (6P64/6P53B + 5%TCP) etched with 5 vol % HF acid for 15 s. No reaction layer can be observed between the calcium phosphate particles and the glass.

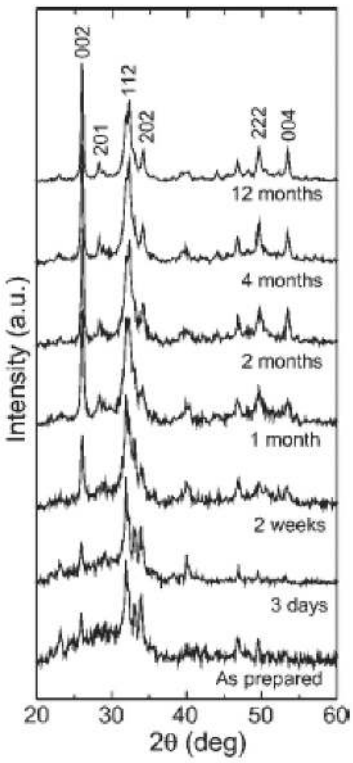

Figure 7.
XRD diffraction patterns of the surface of sample S1 after immersion in SBF for up to 12 months. The main crystalline phase is carbonated hydroxyapatite [HCA, $Ca_{10}(PO_4)_3(CO_3)_3(OH)_2$)], whose peaks are indexed on the figure. The relative intensity of the peaks suggests that the crystals are growing with the c-axis oriented preferentially perpendicular to the coating surface.

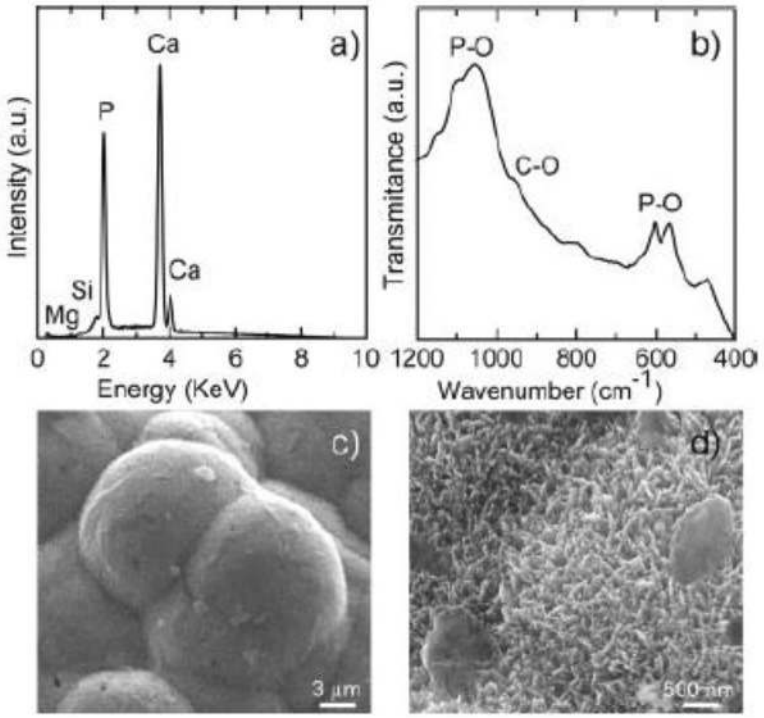

Figure 8.

EDS analysis (a), FTIR analysis (b), and SEM micrographs (c and d) of the apatite crystals precipitated on the surface of S1 (6P64/6P53B + 5% HA) after 4 months in SBF. The FTIR analysis shows the characteristic HCO_3^- vibration bands corresponding to carbonated hydroxyapatite (HCA).

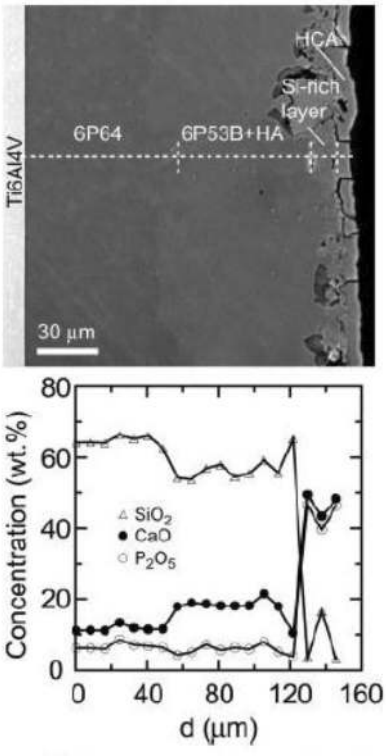

Figure 9.
SEM micrograph and associated EDS line analysis of a cross-section of S1 after 1 month in SBF.

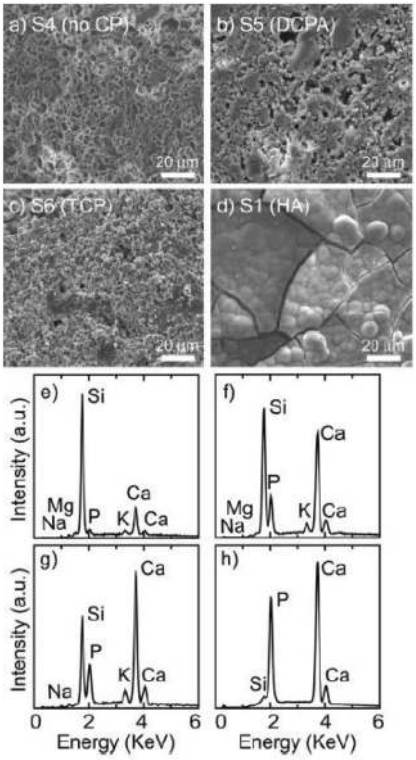

Figure 10.
SEM micrographs (a–d) and EDS analysis (e–h) of the surface of samples S1, S4, S5, and S6, respectively, soaked in SBF for 1 month. Apatite has precipitated on the coatings with synthetic HA particles, whereas only different degrees of glass corrosion and dissolution can be observed in samples with DCPA, β-TCP and without CP additions.

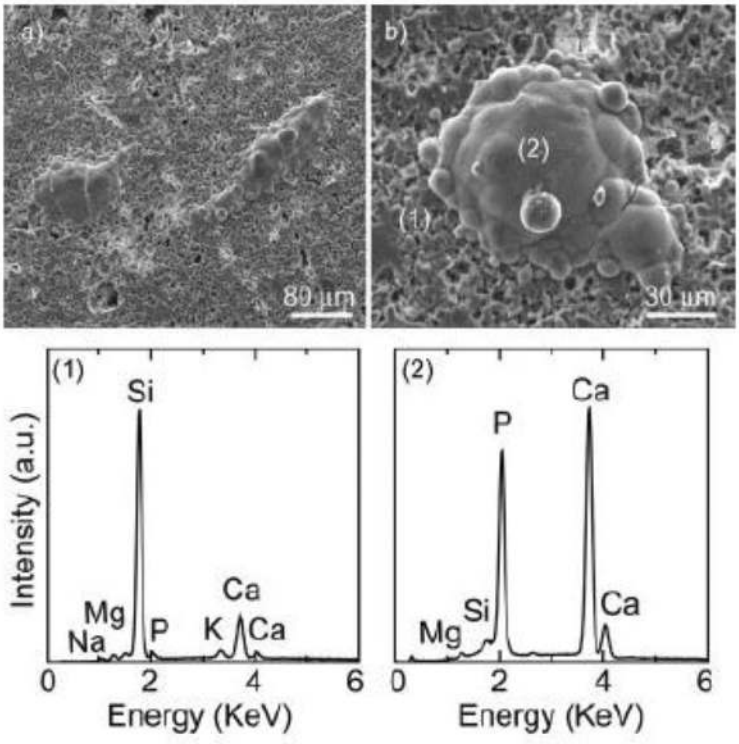

Figure 11.
SEM micrograph of the surface of the coating with no addition of CP particles (S4) after being soaked in SBF for 6 months (a) and detail of isolated precipitate (b). EDS analysis of the surface (1) and a precipitate (2) show that they correspond to glass and apatite, respectively.

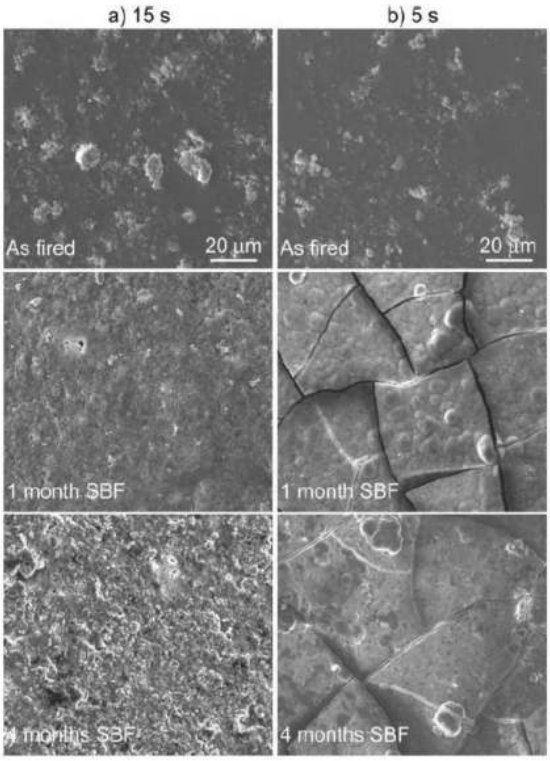

Figure 12.
SEM micrographs of the surface of coatings containing a layer consisting of 6P53B glass and 5 wt % HA fired for 15 s (a) and 5 s (b) at 820°C (S1 and S8, respectively) after immersion in SBF for different times. The coatings exhibit different stages of glass corrosion, but apatite does not precipitate in the samples fired for 15 s. An apatite layer has precipitated in the sample fired for 5 s, where drying cracks are clearly visible.

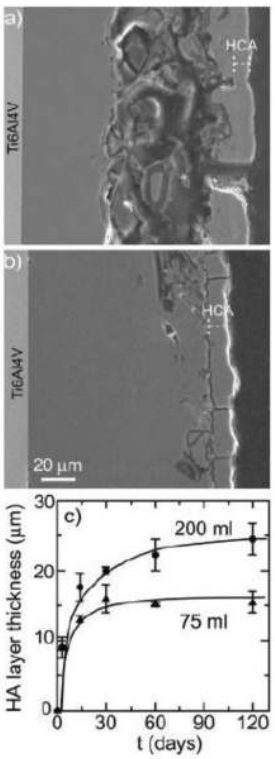

Figure 13.
SEM micrographs of the cross-sections of S1 after being immersed for 1 month in (a) 200 mL SBF and (b) 75 mL SBF. (c) Time evolution of the thickness of the precipitated apatite layer for samples immersed in 75 or 200 mL SBF. Precipitation of apatite stops after 1 month for the sample immersed in 75 mL.

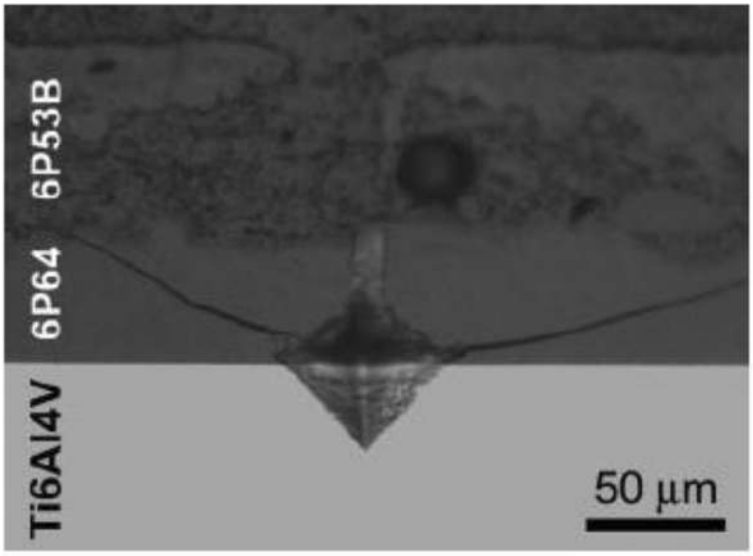

Figure 14.
Vickers indentation performed using a 1-kg load in ambient air at the glass S1/Ti6Al4V interface after soaked in simulated body fluid for 2 months. Even after *in vitro* tests, the cracks do not propagate along the interface, but rather tend to be driven into the glass. The coating did not delaminate qualitatively indicating good glass-metal adhesion. The same behavior was found in all the samples.

Table I

Glass Compositions (in wt %) and Their Thermal Properties

	SiO_2	Na_2O	K_2O	CaO	MgO	P_2O_5	CTE (10^{-6}°C^{-1})	T_g (°C)	T_s (°c)
Bioglas ®	**45**	**24.5**	**0.0**	**24.5**	**0.0**	**6.0**	**15.1**	**511**	**557**
6P50	**49.8**	**15.5**	**4.2**	**15.6**	**8.9**	**6.0**	**12.2**	**522**	**560**
6P53A	**52.7**	**17.0**	**4.6**	**12.6**	**7.1**	**6.0**	**12.9**	**530**	**565**
6P53B	52.7	10.3	2.8	18.0	10.2	6.0	11.5	531	608
6P55	**54.5**	**12.0**	**4.0**	**15.0**	**8.5**	**6.0**	**11**	**548**	**602**
6P57	**56.5**	**11.0**	**3.0**	**15.0**	**8.5**	**6.0**	**10.8**	**557**	**609**
6P61	61.1	10.3	2.8	12.6	7.2	6.0	10.2	564	624
6P64	64.1	9.8	2.7	11.1	6.3	6.0	9.1	565	622
6P68	**67.7**	**8.3**	**2.2**	**10.1**	**5.7**	**6.0**	**8.8**	**565**	**644**

The glasses used in this study have been emphasized in bold. Other glasses have been included for comparison purposes. The coefficient of thermal expansion was measured between 200 and 400°C; T_g is the glass transition temperature and T_S is the softening point.

Table II

Summary of Bilayered Coatings Studied in This Work

Sample	SiO_2 Inner Glass (wt %)	SiO_2 Outer Glass (wt %)	CP Type	CP(wt %)	Firing Time (s)
S1	64	53B	HA	5	5
S2	61	53B	HA	5	5
S3	64	61	HA	5	5
S4	64	53B	None	0	5
S5	64	53B	DCPA	5	5
S6	64	53B	β-TCP	5	5
S7	64	53B	HA	10	5
S8	64	53B	HA	5	15

Table III

Ion Concentrations of the SBF Used in This Research Compared to That of Human Plasma

	Ion Concentration (m*M*)						
	Na^+	K^+	Mg^{2+}	Ca^{2+}	CI^-	HCO_3^-	HPO_4^{2-}
SBF	142.0	5.0	1.5	2.5	148.8	4.2	1.0
Human plasma	142.0	5.0	1.5	2.5	103.0	27.0	1.0

The solution was buffered at the physiological pH 7.25 at 36.5°C with 50 m*M* trishydroxymethyl aminomethane [$(CH_2OH)_3CNH_2$] and 45 m*M* hydrochloric acid (HCI).